Supplementary Information (SI) for New Journal of Chemistry.

Supplementary Material

$BiVO_4/MoS_2$ n-n heterojunction for enhanced solar-driven seawater antibiotic degradation and photocatalytic hydrogen evolution

Bingyan Ni, Ying Liu, Linlin Zhang*, Jianjun Liao， Xiaodong Zhang, Cheng Li

Key Laboratory of Agro-Forestry Environmental Processes and Ecological Regulation of Hainan Province, School of Environmental Science and Engineering, Hainan University, Haikou,570228, China.

*Address correspondence to:
6962zhanglinlin@163.com (L. Zhang)

2.1. Materials and chemicals

The main reagents used in the experiments wereBismuth nitrate pentahydrate ($Bi(NO_3)_3 \cdot 5\ H_2O$, ≥ 98.5%), ammonium metavanadate (NH_4VO_3, A.R.), triethylamine ($C_6H_{15}N$, A.R.), ammonium molybdate tetrahydrate ($(NH_4)_6Mo_7O_{24} \cdot 4(H_2O)$, ≥ 99%), thiourea ($CH_4N_2S$, A.R.), ethanol ($C_2H_6O$, A.R.), isopropanol ($(CH_3)_2CHOH$, A.R.), ethylenediaminetetraacetate acid disodium salt ($C_{10}H_{14}N_2Na_2O_8$, ≥ 99%), nafion 117 solution and p-benzoquinone ($C_6H_4O_2$, A.R.) were purchased from Aladdin Reagent Company, Ltd (Shanghai, China). Nitric acid (HNO_3, A.R.) was purchased from Haikou Shanghe Biotechnology Co. Ltd (Hainan, China). Triethanolamine ($C_6H_{15}NO_3$, ≥ 98%), tetracycline hydrochloride ($C_{22}H_{24}N_2N_8 \cdot HCL$, A.R.) were purchased from McLean Reagent Co. Ltd. (Shanghai, China) All the reagents were used for the experiments without purification, and the water used for the experiments was deionized water (≥ 18.2 M Ω·cm).

2.2. Photocatalysts preparation

2.2.1. Synthesis of $BiVO_4$

Firstly, 6 mmol NH_4VO_3 and 6 mmol $Bi(NO_3)_3 \cdot 5H_2O$ were dissolved in 50 mL of 2 M dilute aqueous nitric acid solution, and the mixed solution was stirred at 60 °C for 30 min. Meanwhile, triethylamine was added dropwise until the pH of the solution reached 7. The whole reaction mixture was poured into a 100 ml Teflon liner in a stainless steel chamber. The sealed autoclave was kept in an oven at 180 °C for 18 hours. After cooling to room temperature, the residue in the liner was extracted, washed three times alternately with water and ethanol, collected by centrifugation and finally dried at 60 °C. The sample was labelled as BVO[1].

2.2.2. Synthesis of $BiVO_4$@MoS_2 (BM) composites and MoS_2

0.45 g of thiourea and 0.17 g of $(NH_4)_6Mo_7O_{24}\cdot 4(H_2O)$ were dissolved in deionized water (20 mL) and stirred to obtain a clear solution. An appropriate amount of prepared $BiVO_4$ powder (0 g, 1.55 g, 0.775 g, 0.517, 0.388 g, 0.31 g is required for making MoS_2, 10 wt%, 20 wt%, 30 wt%, 40 wt% and 50 wt% BM, respectively) was added to the above mixed solution and stirred vigorously for 30 min. The resulting suspension was sonicated for 30 min and transferred to a stainless steel autoclave. The sealed autoclave was kept in an oven at 180 °C for 18 hours. After cooling to room temperature, the powder was washed three times alternately with deionized water and ethanol, and then dried under vacuum at 60 °C to obtain $BiVO_4$@MoS_2 nanocomposites labelled as x% BM, where x% is the mass fraction of MoS_2 in the $BiVO_4$@MoS_2 nanocomposites (BM), which is 10 wt%, 20 wt%, 30 wt%, 40 wt%. 30 wt%, 40 wt% and 50 wt%. When $BiVO_4$ powder is not added, the product is black powder MoS_2[2].

2.3. Characterizations

The crystal structures were analyzed by Cu-Kα radiation (λ = 1.5406 λ) on an X-ray diffractometer (XRD, Smart Lab, Rigaku, Japan) using, and XRD analysis was performed at a scan rate of 10° min-1 in the 2θ range of 10-90°. Scanning electron microscope (SEM, Verios G4 UC, Thermoscientific, Czech Republic) was used to study the morphology of the samples. Prior to SEM testing, the trace powdered solids were sonicated in ethanol and then dried. Afterwards, the powder was adhered to a conductive gel, gold-plated, and placed in an SEM feeder for sample measurement. The fine morphology and lattice spacing of the samples were observed and analyzed by transmission electron microscopy (TEM, Talos F200X G2, Thermoscientific, Czech Republic) at an accelerating voltage of 200 kV. And elemental distribution of the samples were analyzed by additional energy dispersive spectroscopy (EDS). Prior to TEM testing, a small amount of sample was first sonicated in 3 mL of ethanol to form a suspension. A small amount of the suspension was then dispersed drop-by-drop onto a microgrid, dried, and placed in a sample feeder for observation and testing. The electronic states of the elements on the sample surface were determined by X-ray photoelectron spectroscopy (XPS, Thermoscientific K-Alpha+, USA). The instrument used a monochromated Al Kα light source (hν = 1486 eV) as a radiation source, elemental carbon (C1 s) as a calibration reference, a vacuum better than 2 × 10-6 Pa, and a target power of 300 W. The optical absorption properties of the samples were tested by UV-Vis diffuse reflectance spectroscopy (UV-Vis DRS, Lambda950, PerkinElmer, USA) and the bandgap energy was calculated by the KubelkaMunk (K-M) function. The functional group bonding was characterized by Fourier infrared spectroscopy (FT-IR, IFS 66 V/S, Bruker, Germany) and Raman spectroscopy (Raman, Renishaw, UK). The photoluminescence spectroscopy (PL, F-7000, Hitachi, Japan) with a Ge detector and a 450 W Xenon lamp as excitation source was used to characterize the efficiency of electron-hole complexation and evaluate photocatalytic performance. Reactive oxygen species analysis was performed using electron paramagnetic resonance (ESR, Bruker EMXplus-6/1, Germany). The trapping agent was dimethylpyridine N-oxide (DMPO). The adsorption of N2 at -196 °C was determined by a fully automated specific surface area and porosity analyzer (ASAP 2460, Micromeritics, USA), and the specific surface areas and pore size distributions of photocatalysts were obtained based on the adsorption-desorption curves using the BET method and the BJH calculation. An ultraviolet photoelectron spectrometer (UPS, Source Gun Type: He I, Thermo SCIENTIFIC Nexsa) determined the sample work function and valence band position. At an excitation wavelength of 360 nm, fluorescence

2.4. Electrochemical measurements

The transient photocurrent response properties, electrochemical impedance spectroscopy (EIS) and flat band potentials were measured using a typical three-electrode electrolytic cell and a CHI 660 E electrochemical workstation. First, 5 mg of photocatalyst was ultrasonically mixed with 1.5 mL of isopropanol and 0.15 mL of nafion 117 solution for 30 min, then a small amount of the dispersion was drip-coated uniformly onto the ITO conductive film glass, and each time the ITO conductive film glass was placed into an oven at 60 °C to dry for 5 min. In the three-electrode system, the metal platinum sheet was used as the counter electrode, Ag/AgCl was used as the reference electrode, the conductive film glass coated with photocatalyst was used as the working electrode, and the electrolyte was 0.5 M Na_2SO_4 solution (pH=7). All potentials were harmonized to the standard hydrogen electrode (NHE) potential using the following equation: E(NHE) = E(Ag/AgCl) + 0.197 V. The impedance spectral frequency range was from 0.1 Hz to 20 kHz. Flat band potentials were measured by the electrochemical Mott-Schottky method with a frequency of 1 kHz, BVO voltages in the range of -0.2 to +0.8 V, and MoS_2 voltage range from -1 to +1 V. The transient photocurrent response spectra were obtained by placing the prepared electrodes perpendicularly to a 300 W xenon lamp equipped with a cutoff filter (λ>420 nm) light source and keeping the distance between the electrochemical cell and the light source constant at 10 cm, switching on the xenon lamp at intervals of 30 s, and repeating the process for four cycles.

2.5. Photocatalytic degradation of tetracycline hydrochloride (TCH)

2.5.1. Examining the effects of different TCH concentrations

Six groups of 50 mg 40% BM were accurately weighed and added to 50 mL of filtered seawater (pH=8.3) with TCH concentrations of 5, 10, 15, 20, 25 and 30 mg/L, respectively, and then stirred in the dark for 30 min to reach the adsorption equilibrium. 4 mL of the solution was filtered through a 0.22 μm membrane, and the TCH concentration was determined at 360 nm using a UV-visible spectrophotometer (Aoyi Instruments (Shanghai) Co., ltd, China, Model UV-1800). Subsequently, a 300W xenon lamp equipped with a cutoff filter (λ>420 nm) was switched on, stirring was continued, and the TCH concentration was measured every 30 minutes.

2.5.2. Examining the effects of different ratios of heterojunction

Accurately weigh 50 mg of each photocatalysts and add them to 50 mL of filtered seawater with a TCH concentration of 20 mg/L, respectively. Then perform the same steps as in 2.5.1.

2.5.3. Examining the effects of different light sources

Repeat the experiments of 2.5.2. under different light sources, including imitating sunlight (6W), UV lamp (10W) and 300W xenon lamp equipped with a cutoff filter (λ>420 nm). Meanwhile, filtered seawater (TCH concentration of 20 mg/L) without photocatalyst was used as a blank group.

2.5.4. Examining the effects of different water substrates

Two portions of 50 mg 40% BM were accurately weighed and added to 50 mL of seawater and deionized water with a TCH concentration of 20 mg/L, respectively. Then repeat steps in 2.5.1. Meanwhile, filtered seawater and deionized water without photocatalyst (both with a TCH concentration of 20 mg/L) were used as blank groups. And the above experiments were repeated under UV lamp (10W) and imitating sunlight (6W). Three parallel experiments were conducted and the average of the three results was taken as the final experimental result.

2.5.5. Active species trapping experiments

Reactive oxygen species during TCH degradation were investigated by trapping experiments. Isopropanol (IPA), p-benzoquinone (BQ) and ethylenediaminetetraacetate (EDTA) were used to trap hydroxyl radicals (·OH), superoxide anions ($\cdot O_2^-$) and photogenerated holes (h^+) generated during the reaction, respectively. In 50 mL of filtered seawater mixture containing 50 mg of photocatalyst (40% BM) at a TCH concentration of 20 mg/L, 50 mmol/L of BQ and EDTA and 10% (V/V) of IPA were added, respectively, and then the mixture was magnetically stirred in the dark for 30 min to reach adsorption equilibrium, after which a 300W xenon lamp equipped with a cutoff filter (λ>420 nm) was switched on and stirring was continued for 180 min. After 180 min, TCH concentrations were determined using the same method as in 2.4.1.

2.6. Photocatalytic hydrogen evolution experiments

30 mg of photocatalyst was added to a 60 mL filtered seawater solution containing 15 mL of triethanolamine. The reaction was carried out in a Pyrex top irradiation unit. The photoreactor was then connected to a closed gas cycle for a 30-minute nitrogen-filled pretreatment in dark to ensure that the reactor was under anaerobic conditions prior to the photocatalytic experiments. Subsequently, the solution was irradiated with a 300 W xenon lamp equipped with an Air Mass 1.5 global filter (AM 1.5 G, 100 mW/cm^2). A cooling circulation system was used to control the temperature during the reaction. The amount of hydrogen produced was determined by gas chromatography using a TCD detector. Photocatalytic stability was determined with the same experimental factors.

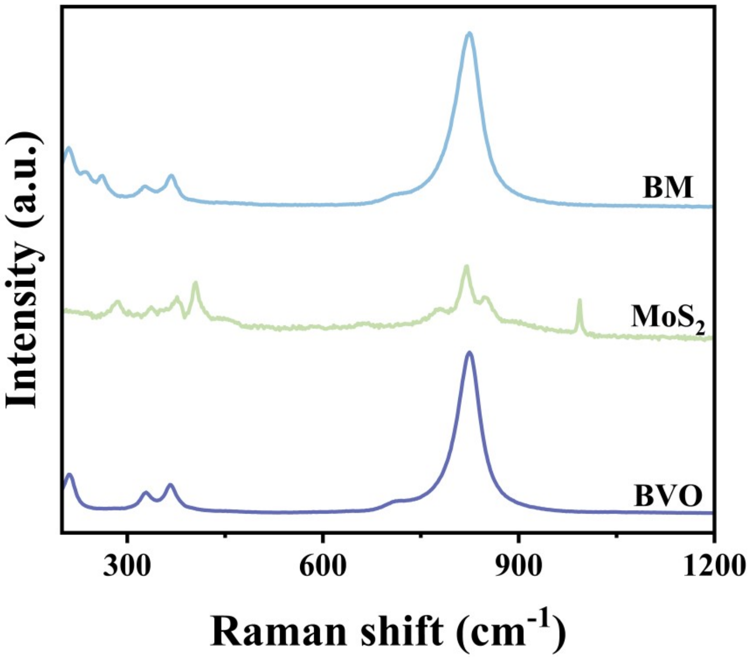

Fig. S1. Raman spectra of MoS_2, BVO and BM.

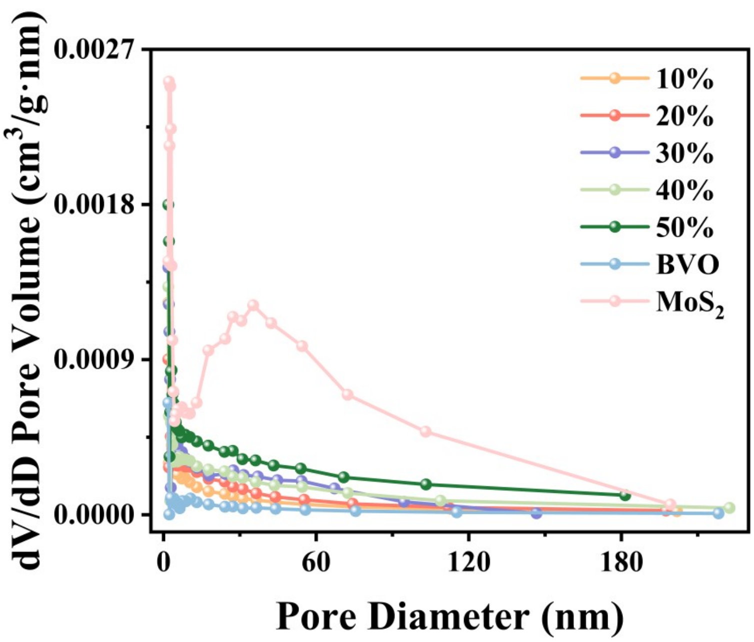

Fig. S2. Pore size distribution curves of photocatalysts.

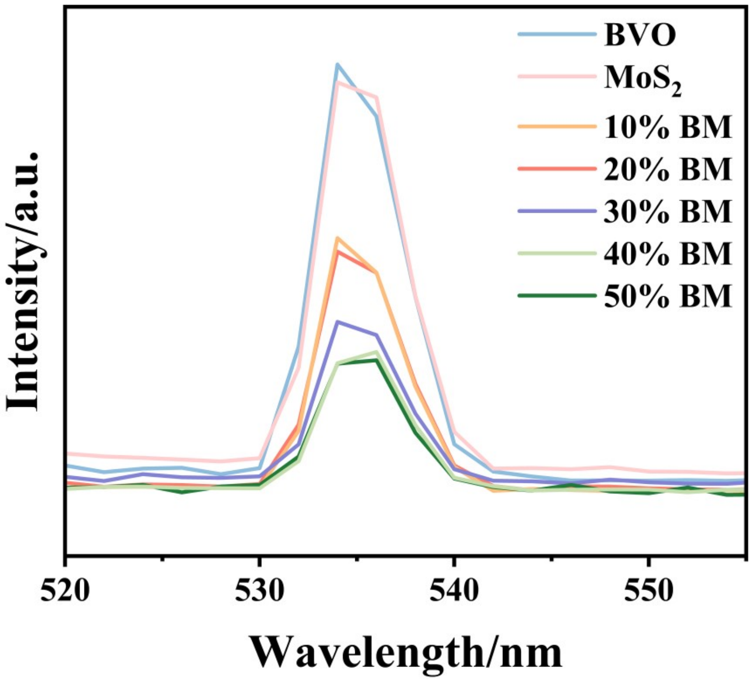

Fig. S3. PL spectra.

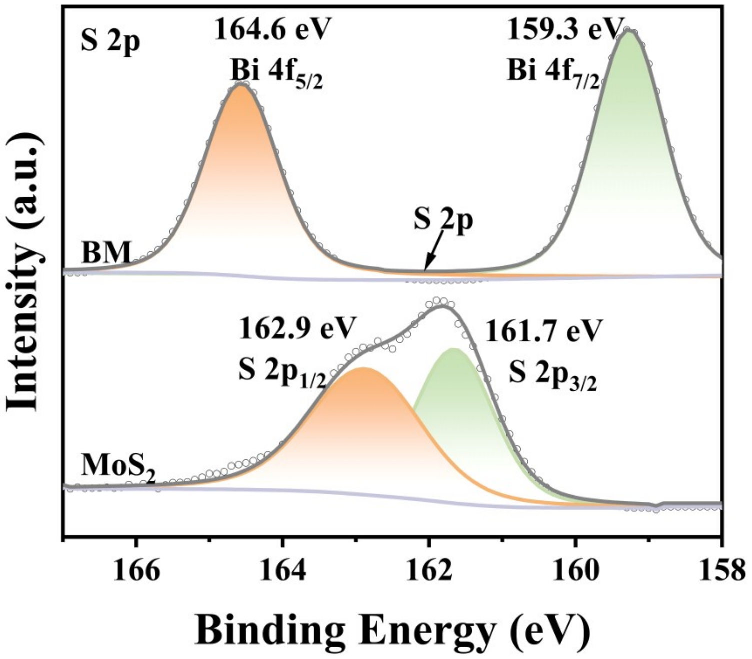

Fig. S4. High-resolution XPS spectra of S 2p in MoS_2 and BM.

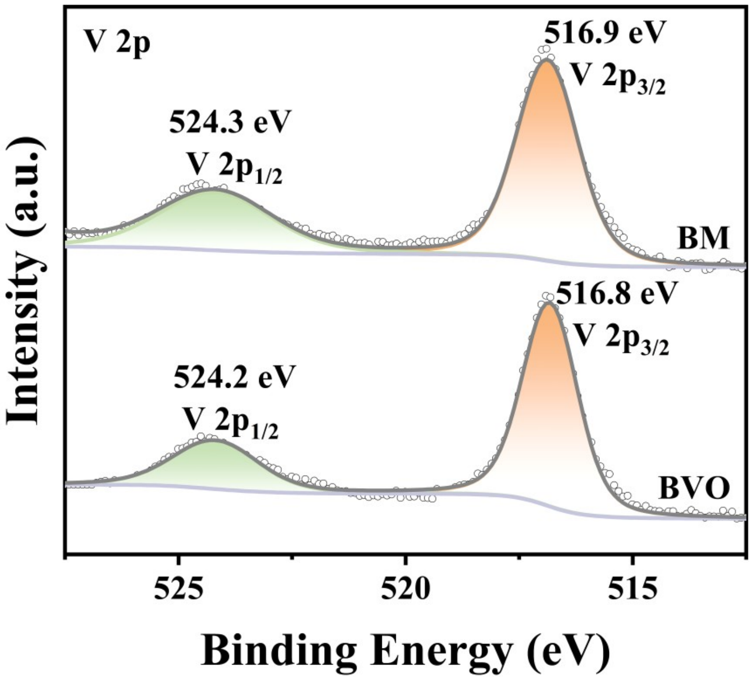

Fig. S5. High-resolution XPS spectra of V 2p in BVO and BM.

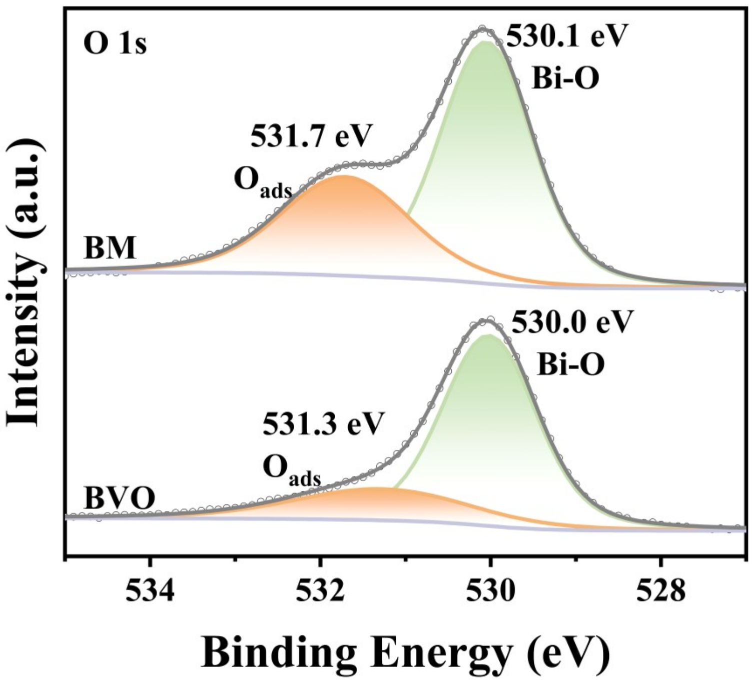

Fig. S6. High-resolution XPS spectra of O 1s in BVO and BM.

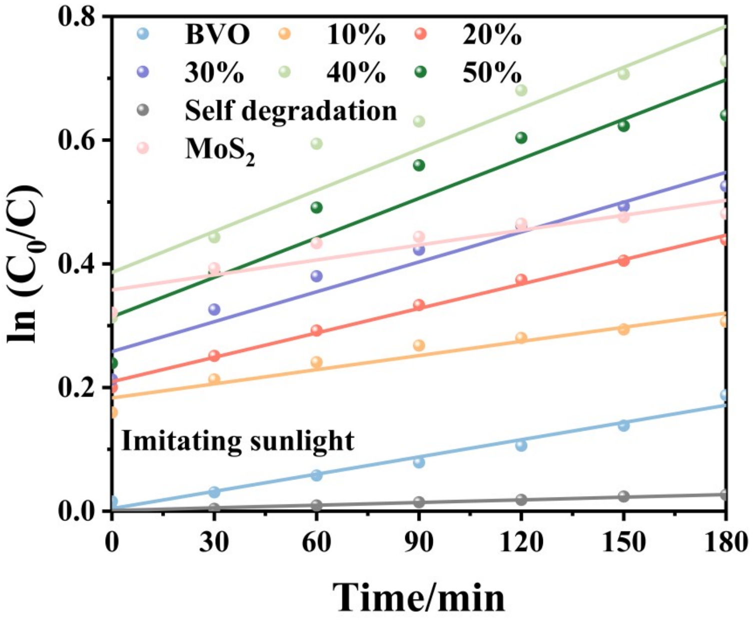

Fig. S7. Kinetic profiles describing the degradation of TCH for different samples under sunlight imitation (seawater).

Table S1. Slope and variance of the kinetic curve of the samples

	Self-degradation	**BVO**	**MoS_2**	**10%BM**	**20% BM**	**30% BM**	**40% BM**	**50% BM**
k	0.00014	0.00093	0.00080	0.00076	0.00132	0.00161	0.00221	0.00213
R^2	0.9852	0.9674	0.8148	0.9053	0.9935	0.9296	0.8531	0.8572

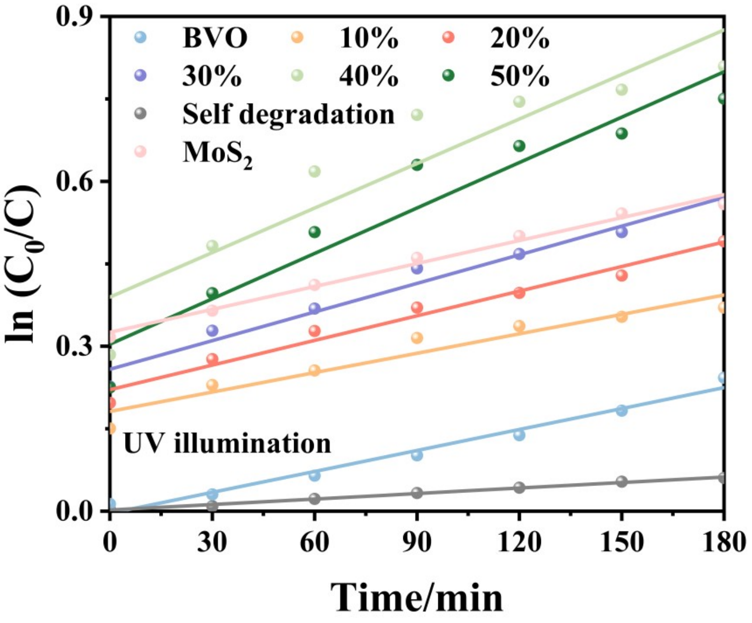

Fig. S8. Kinetic profiles describing the degradation of TCH for different samples under UV illumination (seawater).

Table S2. Slope and variance of the kinetic curve of the samples

	Self-degradation	**BVO**	**MoS_2**	**10%BM**	**20% BM**	**30% BM**	**40% BM**	**50% BM**
k	0.00033	0.00127	0.00139	0.00118	0.00149	0.00174	0.00275	0.00270
R^2	0.9922	0.9746	0.9850	0.9151	0.9692	0.9643	0.8341	0.8959

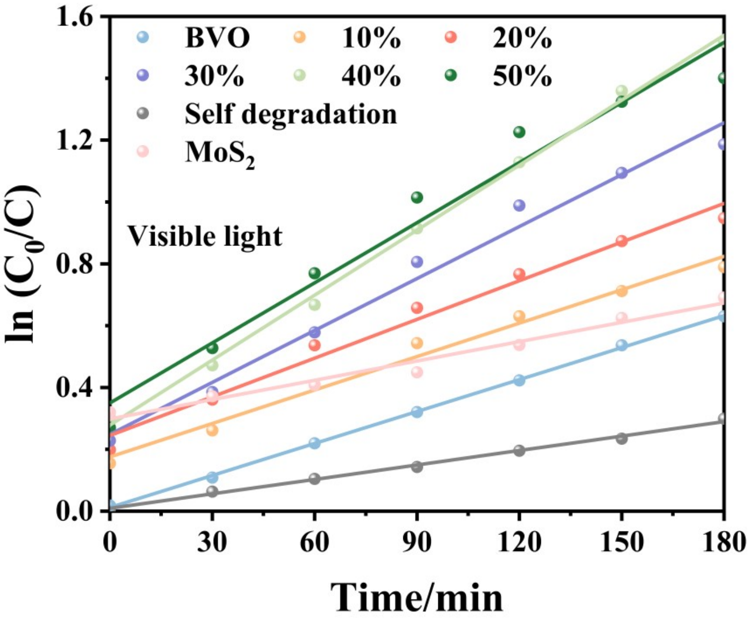

Fig. S9. Kinetic profiles describing the degradation of TCH for different samples under visible light (seawater).

Table S3. Slope and variance of the kinetic curve of the samples

	Self-degradation	**BVO**	**MoS_2**	**10%BM**	**20% BM**	**30% BM**	**40% BM**	**50% BM**
k	0.00156	0.00345	0.00208	0.00360	0.00417	0.00560	0.00700	0.00648
R^2	0.9948	0.9993	0.9701	0.9825	0.9783	0.9792	0.9968	0.9590

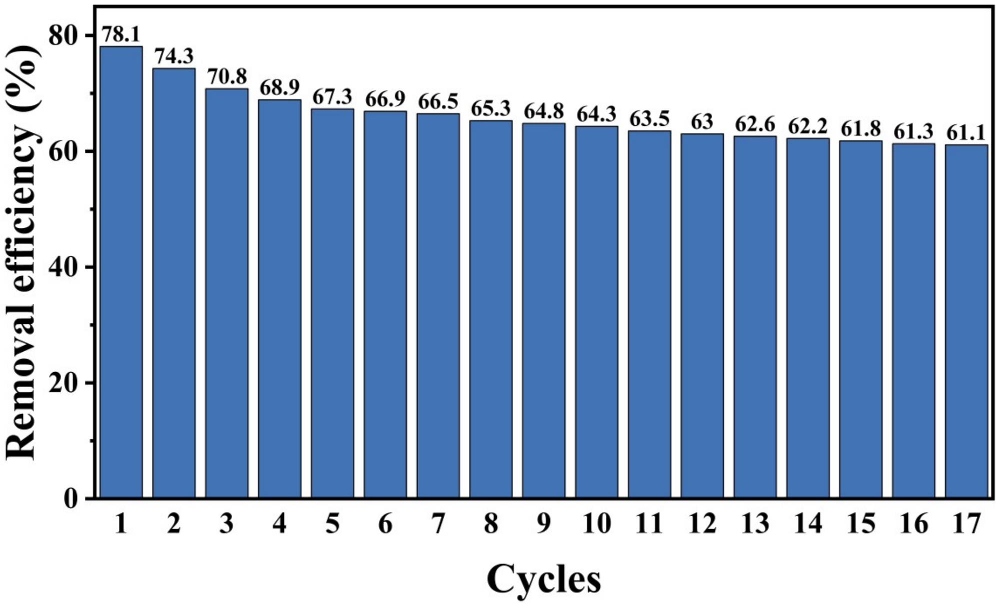

Fig. S10. Cycle experiments (51h) for photodegradation of TCH over 40% BM.

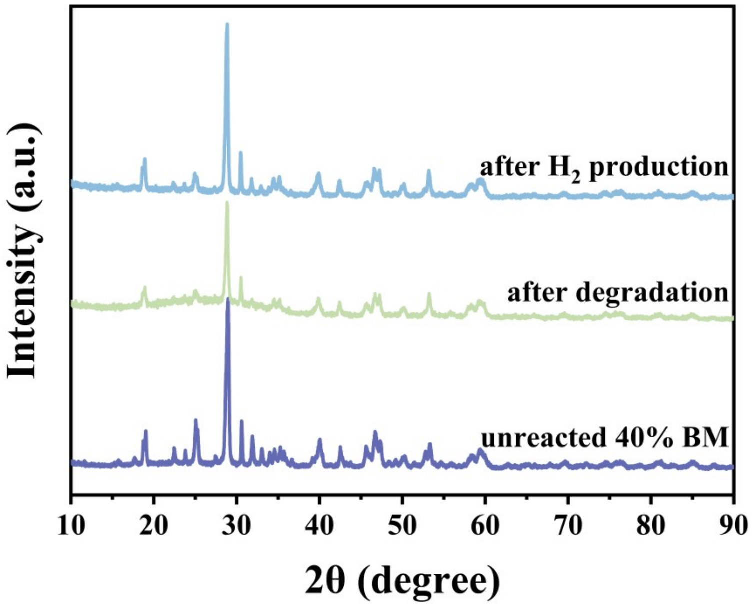

Fig. S11. XRD patterns before and after hydrogen production and degradation.

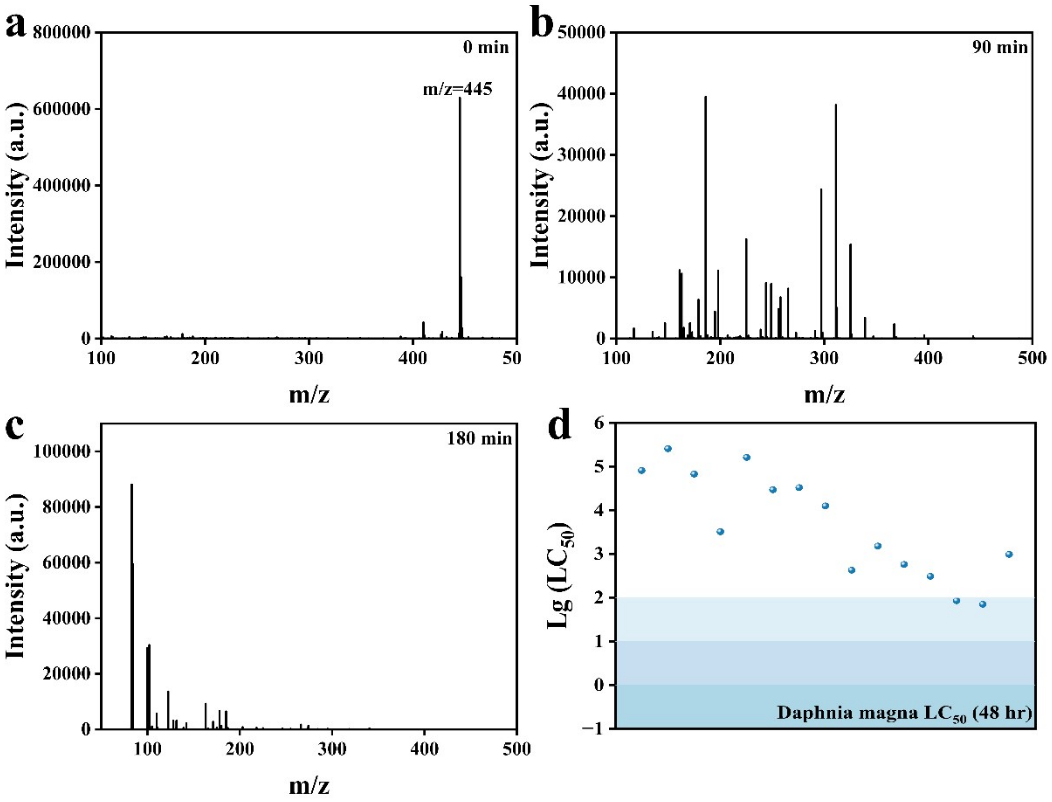

Fig. S12. LC-MS profiles of intermediates of TCH (a-c) and Predicting the toxicity of pollutants and their transformation products (d).

Table S4. Toxicity classification according to the Globally Harmonized System of Classification and Labelling of Chemicals[3].

Toxicity range (mg/L)	**Logarithmic-transformed toxicity range**	**Classification**
LC50[a]/EC50[b]/ChV[c] ≤ 1	lg (LC50[a]/EC50[b]/ChV[c]) ≤ 0	Very toxic
$1 <$ LC50/EC50/ChV ≤ 10	$0<$ lg (LC50/EC50/ChV) ≤ 1	Toxic
$10 <$ LC50/EC50/ChV ≤ 100	$1<$ lg (LC50/EC50/ChV) ≤ 2	Harmful
LC50/EC50/ChV > 100	lg (LC50/EC50/ChV) > 2	Not harmful

[a] LC50, Half lethal concentration; [b] EC50, Half effective concentration; [c] ChV, Chronic toxicity value.

Table S5. Comparison of photocatalytic degradation of antibiotics.

Photocatalysts	**Antibiotics**	**Light Source**	**Experimental conditions**	**degradation efficiencies**	**Refs.**
MnO_2/ $BiVO_4$	TC	50W halogen lamp (λ>420nm)	aqueous solution (0.5 g/L TC)	59% (120min)	4
$BiVO_4$/ α-Fe_2O_3	TC	300W Xe lamp (λ>420nm)	aqueous solution (20 mg/L TC)	75.8% (120min)	5
MoS_2/ $PbTiO_3$	TC	300W Xe lamp (λ>420nm)	aqueous solution (50 mg/L TC)	76.97% (180min)	6
Bi/Bi_2S_3- $BiVO_4$	TCH	300 W Xe lamp (λ>420 nm)	aqueous solution (10 mg/L TCH)	78% (120min)	7
$BiVO_4$/ rGH	TCH	300 W Xe lamp	aqueous solution (10 mg/L TCH)	73.2% (120min)	8
MoS_2/ $BiVO_4$	TCH	300W Xe lamp (λ>420nm)	natural seawater (20 mg/L TCH)	78.1% (180min)	This Work
			aqueous solution (20 mg/L TCH)	84.5% (180min)	

Table S6. Comparison of hydrogen evolution rate.

Photo catalysts	**Light Source**	**Reaction Conditions**	**H_2 Evolution Rate (μmol·g^{-1}·h^{-1})**	**Refs.**
rGO/ TiO_2	Philips PL-S 9W lamp	synthetic seawater (20% methanol)	1.6	[9]
NiO/nano-TiO_2	300 W Xe lamp	synthetic seawater (50 mM oxalic acid sacrificial reagent)	0.292	[10]
GaP-C3N4	300 W Xe lamp（AM 1.5G）	artificial seawater	8	[11]
h-$BiVO_4$ /RGO	200 W Hg-Xe arc lamp (λ>420 nm)	aqueous solution (1 vol.% ethanol)	11.5	[12]
Ta_2O_5/ $BiVO_4$	300 W Xe lamp（AM 1.5G）	aqueous solution (0.03/0.12 mol L^{-1} solution of Fe^{2+}/Fe^{3+} ions)	3.4	[13]
MoS_2/ In_2O_3	300 W Xe lamp	aqueous solution (10mg/L RhB)	0.9	[14]
$BiVO_4$/ MoS_2	300 W Xe lamp（AM 1.5G）	Natural seawater (25 vol.% TEOA)	0.27	This Work

Table S7. Stability Comparison of H_2 evolution efficiency.

Photocatalysts	**Number of cycles**	**activity retention rate**	**Reaction Conditions**	**Refs.**
$Pt/A\text{-}TiO_2$	3 (30h)	45.9%	Simulated seawater	[15]
TiO_2/RuO_2	4 (12h)	81%	simulated seawater (30 vol.% methanol)	[16]
$Pt/GaP\text{-}C_3N_4$	4 (16h)	82%	artificial seawater	[11]
$p\text{-}NiSe_2$	5 (25h)	42.9%	Aqueous (10 vol.% TEOA)	[17]
$BiVO_4/MoS_2$	3 (48h)	81%	Natural seawater (25 vol.% TEOA)	This Work

Table S8. The interfacial charge transfer resistance for different materials.

Materials	MoS_2	BVO	10%BM	20%BM	30%BM	40%BM	50%BM
R_{ct}/Ω	281290	50022	42068	11951	19291	8402	8712

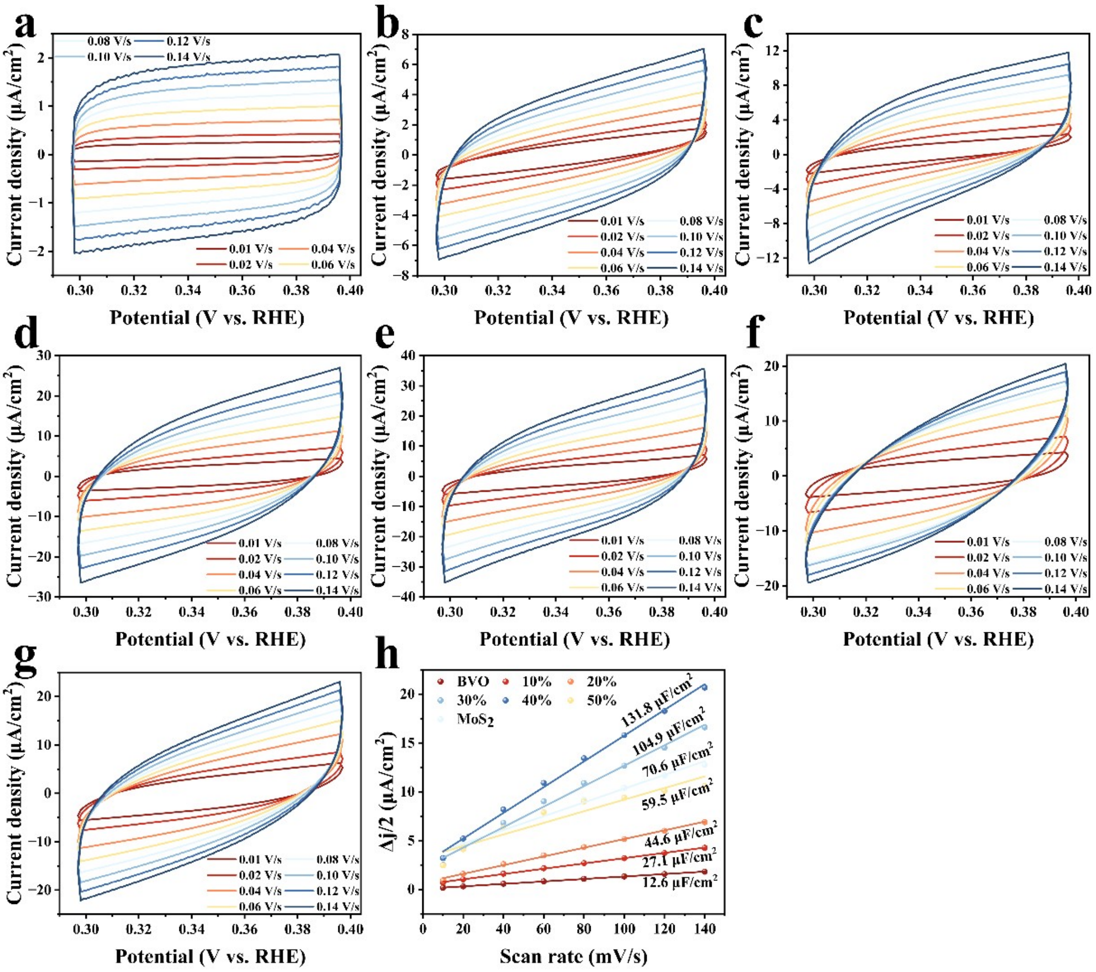

Fig. S13. Cyclic voltammograms of BVO (a), 10%BM (b), 20%BM (c), 30%BM (d), 40%BM (e), 50%BM (f), MoS_2 (g) and their corresponding C_{dl} values (h).

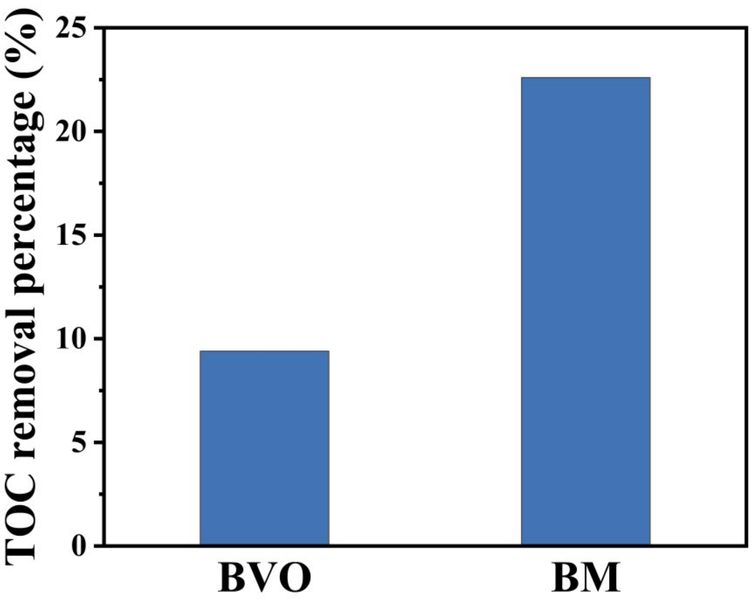

Fig. S14. TOC removal ratio of TCH by BVO and 40% BM in natural seawater.

References

1. S. Deka, M. B. Devi, M. R. Khan, n. Keerthana, A. Venimadhav and B. Choudhury, *ACS Applied Nano Materials*, 2022, DOI: 10.1021/acsanm.2c02072.
2. R. Du, K. Xiao, S. He, Y. Wang and C. Kang, *Journal of Alloys and Compounds*, 2023, **955**, 170168.
3. S. Jia, H. Han, B. Wang, J. Liu, Q. Tang, G. Liu, Q. Ruan, X. Zhu, H. Li, C. Wang, P. K. Chu and Y. Hua, *Applied Catalysis B: Environment and Energy*, 2024, **353**, 124050.
4. M. Liaqat, N. R. Khalid, M. B. Tahir, S. Znaidia, H. Alrobei and M. Alzaid, *Ceramics International*, 2023, **49**, 10455-10461.
5. C. Ma, J. Lee, Y. Kim, W. Cheol Seo, H. Jung and W. Yang, *Journal of Colloid and Interface Science*, 2021, **581**, 514-522.
6. Z. Dong, Z. Wang, T. Yang, H. Feng, L. Li, I. Ullah and S. Xue, *Colloids and Surfaces A: Physicochemical and Engineering Aspects*, 2024, **683**, 133096.
7. X. Fan, H. Liang, M. Zhang, C. Li and J. Bai, *Colloids and Surfaces A: Physicochemical and Engineering Aspects*, 2025, **707**, 135929.
8. C. Ma, W. C. Seo, J. Lee, Y. Kim, H. Jung and W. Yang, *Chemosphere*, 2021, **275**, 130052.
9. J. Corredor, E. Perez-Peña, M. J. Rivero and I. Ortiz, *Membranes*, 2020, **10**, 218.
10. A. J. Simamora, F.-C. Chang, H. P. Wang, T. C. Yang, Y. L. Wei and W. K. Lin, *International Journal of Photoenergy*, 2013, **2013**, 419182.
11. H. V. Dang, Y. H. Wang and J. C. S. Wu, *Applied Surface Science*, 2022, **572**, 151346.
12. K. Sekar, A. Kassam, Y. Bai, B. Coulson, W. Li, R. E. Douthwaite, K. Sasaki and A. F. Lee, *Applied Materials Today*, 2021, **22**, 100963.
13. H. Gonçalves, D. Freitas, E. Souza, M. Melo, J. Gonzalez-Moya, E. Padrón-Hernández, S. Khan and G. Machado, *Journal of the Brazilian Chemical Society*, 2022, DOI: 10.21577/0103-5053.20220002.
14. Y. Hong, L. Yang, Y. Tian, X. Lin, E. Liu, W. Sun, Y. Liu, C. Zhu, X. Li and J. Shi, *Journal of the Taiwan Institute of Chemical Engineers*, 2023, **146**, 104862.
15. Z. Zhao, W. Li, Y. Wang, J. An, Q. He, S. Zhan and F. Zhou, *International Journal of Hydrogen Energy*, 2025, **109**, 1055-1063.
16. H. Li, B. Zhu, J. Sun, H. Gong, J. Yu and L. Zhang, *Journal of Colloid and Interface Science*, 2024, **654**, 1010-1019.
17. J. Yi, Z. Zhou, Y. Xia, G. Zhou, G. Zhang, L. Li, X. Wang, X. Zhu, X. Wang and H. Pang, *Chinese Chemical Letters*, 2023, **34**, 108328.